GNSS-IR Inshore Tide Measurement Based on Low-cost Chipset

Jie Li, Dongkai Yang, Feng Wang and Jin Xing
BeiHang university

Abstract: Multipath signals that impact positioning accuracy are progressively being utilized to recover land and ocean geophysical information with the introduction of Global Navigation Satellite Systems (GNSS). An interference signal-based approach is GNSS-interferometry reflectometry (GNSS-IR). In this work, interference signals are gathered for sea surface altimetry using a low-cost GNSS signal receiver outfitted with a right-handed circularly polarized antenna, which can reduce cost of tide measurement. This study decompose the raw signal-to-noise ratio and extracts several frequency components using an empirical mode decomposition technique. The vertical distance between the antenna phase center and the sea surface is then calculated using Lomb-Scargle periodogram after the spectra of various frequency components has been analyzed. The final inversion tide is then obtained by removing the wild spots using the sinusoidal fitting approach. According to the results, there is a 0.89 correlation between the measured and recovered tides, and the RMSE is 0.23 m.

Keywords: global navigation satellite systems interferometry reflectometry, tide, empirical mode decomposition, sinusoidal fitting

1. Introduction

Reliable inshore tide measurements are crucial for tourism, dock operations, and fisheries production[1]. Tide measurement stations, which are costly to build, are one of the conventional techniques of monitoring the tide[2]. With the benefits of extensive coverage, excellent accuracy, and no

identifiable signal source, GNSS-IR altimetry uses reflected signal path delay to calculate height[3]. GNSS-IR has been used in the retrieval of soil moisture[4], measurement of vegetation growth state[5], measurement of snow depth[6], and measurement of lake level[7].

In 1993, Martin-Neira developed the Passive Reflectometry and Interferometry System (PARIS) idea and employed interference signals created by direct and reflected signals from the sea surface to estimate sea surface height[8]. Based on the PARIS idea, Martin-Neira et al. conducted a GPS-R sea surface height measuring experiment in Amsterdam in 1997, and the outcomes supported the viability of obtaining sea surface height from satellite navigation signals[9].

GNSS-IR has been widely used to measure tides. A technique based on wavelet analysis and least squares estimate was presented by Wang et al. to rectify the arc height variation inaccuracy of a single SNR[10]. They used a location in Hong Kong, China, to evaluate the method's capacity to take height fluctuation error into account and prevent mistake inheritance. A signal processing-based quality control approach is suggested to handle LSP graphs with several comparable peaks. This approach combines a number of criteria with outside limitations. According to experimental results, this approach can successfully lower gross error and improve measurement accuracy[11]. From 2008 to 2020, Peng et al. installed GNSS observation stations in three coastal regions with various land motions to assess the sea surface height. Results indicate that, when

compared to *in-situ* tidal, the precision of daily mean sea surface height measurements is less than 1.5 cm, and the trend in time is comparable with *in-situ* tidal within the uncertainty range[12]. At Thule, Greenland, which is frequently impacted by icebergs and sea ice throughout the year, an experiment was carried out. The estimated uncertainty is 18 cm, however the root means square deviation (RMSD) is 13 cm[13]. A coherent integration time optimization model was created[14] in order to more accurately forecast how the accuracy of GNSS-IR altimetry varies with coherent integration time and eventually improve altimetry accuracy.

Due to the complicated sea conditions, sea waves and undercurrents may create several frequency components of GNSS interference signals, decreasing measurement accuracy. In order to investigate and perhaps address the multi-frequency mixing problem, researchers use signal processing techniques. By reducing the function of signal-to-noise ratio (SNR) noise, increasing the measurement accuracy of multipath frequency extracted from SNR data by Lomb-Scargle periodogram (LSP), and other methods, Wang et al. found that discrete wavelet decomposition can improve the performance of tide measurement[15]. The researchers then made the suggestion that in order to solve the problem that the elevation angle of the satellite significantly affects the tidal inversion of the GNSS interferometric signal, one could use the EMD technique to decompose SNR in order to produce an effective SNR residual sequence. They utilized data from the American SC02 and Australian RSBY databases to confirm the results[16]. The results show that EMD boosts GNSS data use and expands the range of GNSS interference signals that are usable. Hu et al. proposed a novel GNSS-IR tidal estimating model combined with variational mode decomposition (VMD)[17] using measured data from Sweden's Onsala Space Observatory. The results show that the model improves stability and accuracy, with a correlation value that can be close to 0.97.

This work employed a low-cost GNSS receiver to gather interference signals in order to lower the cost and increase the coverage of shore tidal monitoring.

Many diffuse processes, such as waves and the roughness of the ocean surface, produce reflected signals with various frequency ranges. The raw interference signal was divided in this study using the empirical mode decomposition (EMD) method to produce the reflected signal with various frequencies as well as the DC component (direct signal). The spectrum of the reflected signals at various frequencies is then calculated using the LSP spectrum estimate technique. This work uses the sinusoidal fitting approach to fit the recovered sea surface height and removes the points with a large modulus from the fitting function since tidal fluctuation tends to be a sine function. The rest of this essay is organized as follows: The GNSS-IR sea level measurement theoretical premise is introduced in the second section. The experimental verification is done in the third section. The results are shown in the fourth section. The conclusion of the study is elaborated in the final section.

2. Methodology

Signals reflected by the sea surface can also be picked up by GNSS devices in addition to direct signals. Sea levels can be determined due to the knowledge about the sea surface contained in these reflected impulses. The electromagnetic pulse can be viewed as a plane wave given the great distance between land-based GNSS receivers and spacecraft. The layout of GNSS-IR altimetry is shown in Figure 1, and the total of the red lines represents the route delay between the reflected and direct signal.

The path delay of the direct reflection signal can be determined using the geometric correlations in Figure 1 as follows:

$$\delta = \frac{h}{\sin\theta} - \frac{h}{\sin\theta}\cos 2\theta \qquad (1)$$

where h represents the height of the GNSS antenna and θ represents the satellite elevation angle. After simplified, Equation (1) can be written as:

$$\delta = 2h\sin\theta \qquad (2)$$

The oscillation frequency of the interference signal with the satellite elevation angle sine as the

horizontal axis is:

$$f = \frac{d(\delta/\lambda)}{d \sin\theta} = \frac{2h}{\lambda} \tag{3}$$

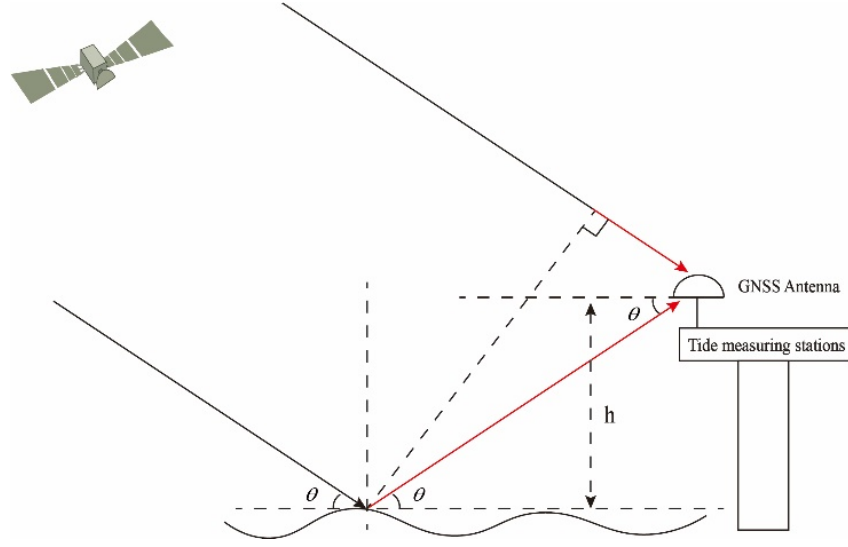wherein λ represents the wavelength of electromagnetic wave.

Figure 1 Geometry of GNSS-IR altimetry

Equation (3) states that the vertical separation between the antenna and the reflector determines the fluctuation frequency of the interference signal, which in turn relies on the height of the GNSS antenna. As a result, the sea level can be determined using the aforementioned hypothesis.

Due to the complicated nature of sea circumstances, reflected signals will have a range of various frequency components. The reflected signals from various reflectors should be successfully retrieved before height measurement. The signal is broken down into the total of several intrinsic mode functions using an approach known as empirical mode decomposition (EMD), which bases its time scale on the local features of the signal (IMF). EMD successfully extracts the feature information from the original signal while emphasizing the local characteristics of the reflected signals.

Signals that are reflected off the sea surface interact with direct signals; the interference signal's SNR is represented as:

$$SNR = A_d^2 + \sum_{i=1}^{n}(A_i^2 + A_d A_i \cos\varphi_i) \tag{4}$$

wherein A_d represents the amplitude of the direct

signal, A_i represents the amplitude of i-th reflected signals, and φ_i represents the phase difference between direct and i-th reflected signals. According to the EMD theory, A_d is the residual component after the decomposition of n IMF components, the oscillating terms are different IMFs.

The processing of EMD is shown in Figure 2:

1) Initialization: $r(t) = x(t)$, $i = 0$, $k = 1$, the termination threshold condition is $\sigma = 0.2\sim0.3$, where $x(t)$ represents the raw SNR data, i means the number of iterations, and k means the serial number of IMF.

2) The local maximum and minimum points of $r(t)$ obtained; The upper and lower envelope $e_{max}(t)$ and $e_{min}(t)$ of the signal were obtained by fitting the maximum and minimum points respectively with cubic spline curves. The average envelope $m(t)$ was obtained by calculating the local mean values from the upper and lower envelope.

3) Let $i = i+1$, subtract the mean envelope from the raw signal to get the component to be identified:

$$p_i(t) = r(t) - m(t) \qquad (5)$$

4) Calculate the termination iteration condition SD. It is generally impossible to completely realize the mean value of the upper and lower envelope to be 0. Normally, if $SD < \sigma$, let $IMF_k(t) = p_i(t)$ and go to the next step, or let $r(t) = p_i(t)$ and repeat the step (2)-(4).

5) Calculate $r(t) = r(t) - IMF_k(t)$, and Determine whether $r(t)$ is monotonic. If it is not, return to step (2) and execute $k = k + 1$ until $r(t)$ is a monotonic function. The final signal is decomposed into the following forms as Equation (4).
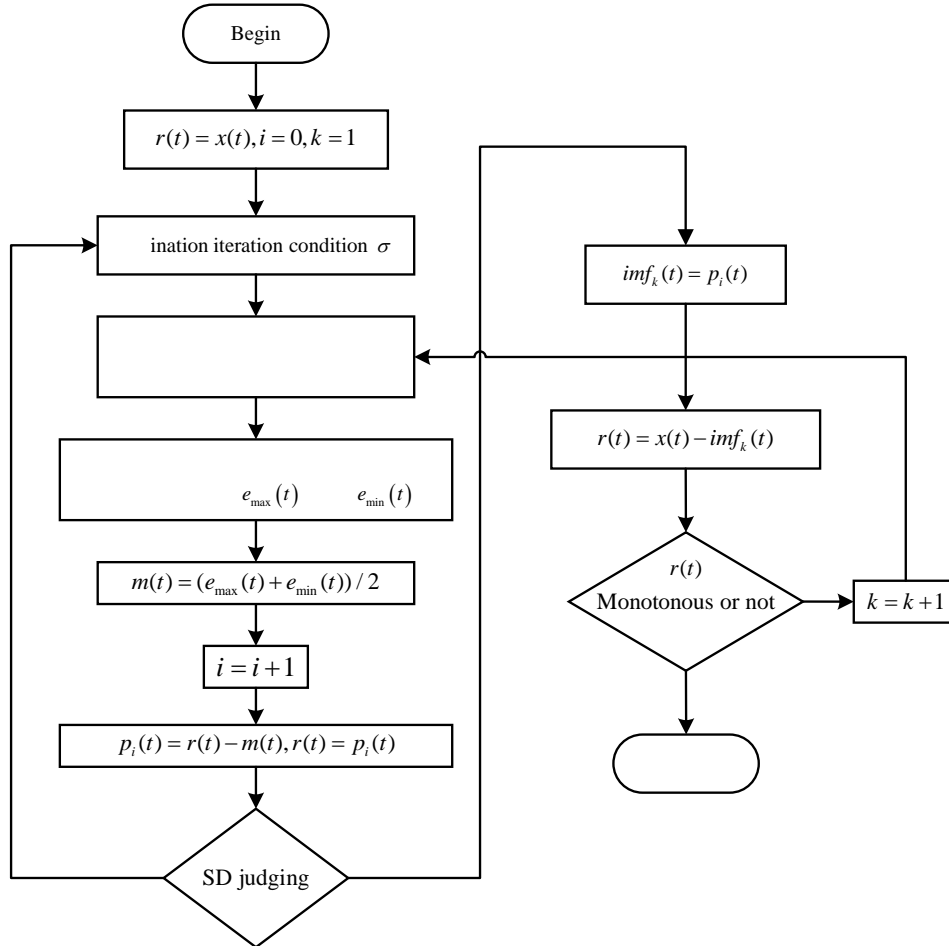

Figure 2 EMD flow diagram

Similar frequency components may still be present in the partial IMF following EMD decomposition, and the predicted and actual sea surface heights will vary significantly. This research used sinusoidal function fitting to acquire observed tidal trends and eliminate the wild areas because tides exhibit a sinusoidal trend. When there is a storm surge or a powerful sea surface breeze, the variation in sea level that GNSS-IR detects deviates from the sinusoidal rhythm. This part of the data can be marked as "unreliable" and excluded because GNSS-IR is presently unable to identify ocean height

with any degree of reliability. Furthermore, if the data deviates from the sinusoidal pattern even for a short while, the sea surface might be having storm surge. This forecast method can be used as a new area of investigation in this study.

In this research, RHCP antenna is utilized. The primary polarization features of the reflected signal will change to LHCP when the satellite elevation angle is larger than the Brusset angle[1]. In this research, a scenario was run under the following circumstances: The tide height is and the distance between the GNSS station and sea level is 8 meters.

The modeling of interfering signal SNR is depicted in Figure 3. Low satellite height angles cause the SNR to clearly fluctuate. Additionally, the SNR fluctuates significantly due to the intricacy of the sea surface.

We decomposed the raw SNR using the EMD method, and the outcomes are depicted in Figure 4. The five panels on the right depict the corresponding LSP spectrum, while the five panels on the left show the IMF components (IMF1,4,5,6, and 7). The

simulation results demonstrate that the EMD initially breaks down to produce high-frequency components before progressively decreasing in frequency. The sea surface reflects a large number of messages with high-frequency components. The height recorded by IMFs IMF5 and IMF6 should be the vertical distance between the GNSS antenna and sea surface, however, as the low-frequency component's highest value is around 8 m.
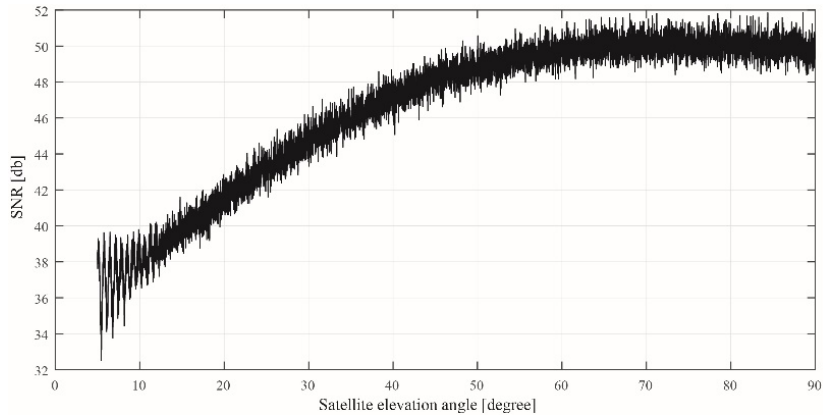

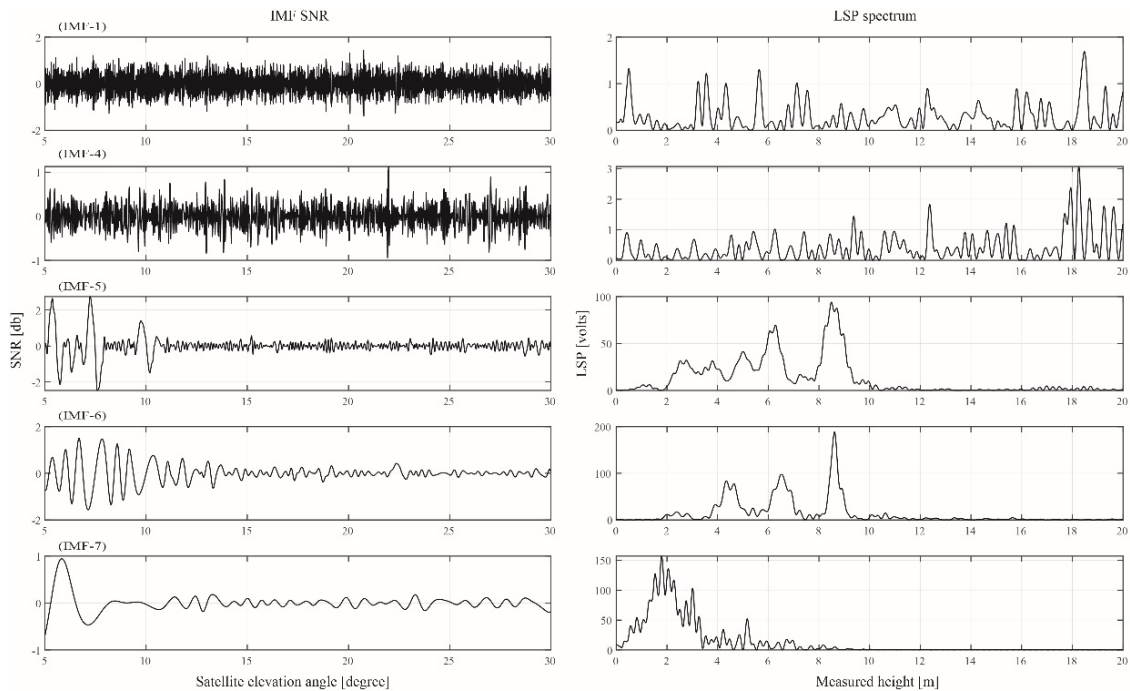Figure 3 Simulation of interference signal SNR

Figure 4 Simulation of IMF and LSP spectrum for raw interference signal SNR

The signal still contains frequency components after EMD that cannot be distinguished. In this investigation, anomalous inversion values were eliminated using sine fitting. Figure 4 displays two

almost equal peaks for IMF-5 and IMF-6, which should be noted since they will affect the measurement. An IMF with a high peak power was employed for this experiment.

96

Figure 5 displays the results, with the measured height shown by the star mark, the fitting curve displayed by the black solid line, and the correct height indicated by the blue dashed line. It can be
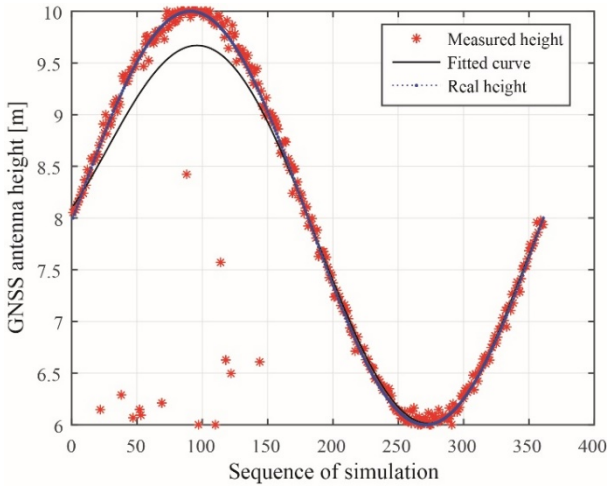

Figure 5 Simulation of measured and real height

3. Experiment

We conducted an experiment at Qingdong 5 tide measurement station in Dongying, Shandong Province. The location is 20 kilometers from eastern shoreline, the long-term sea breeze is mild, but there could be a brief storm surge. The coordinate of the station is ($37°26'51''N, 119°0'36''E$), and the experiment period is November 2021. The GNSS antenna was installed towards the southwest, which is nearly 7m above the sea surface. The receiver was placed in a waterproof iron box, and the raw SNR of GNSS interference signal is recorded as a sample rate of 1s. The experiment site was shown in Figure 6, (a) is the experiment station, (b) is the ron box, (c) is the the GNSS antenna, and (d) is the low-cost GNSS chipset.

The satellite elevation angle is labeled on Figure 7 as the X-label, and the interference signal's raw SNR is labeled on the Y-axis. The SNR of the raw interference signal oscillates when the satellite's elevation angle is low. The oscillation vanishes when the satellite's elevation angle rises, which is consistent with the outcomes of the simulation. Therefore, in the data processing of this study, only the satellite elevation angle 5° to 25°, and azimuth 120° to 280° was selected.

Similarly, EMD are used to decompose various

regarded as a wild point and eliminated when the modulus between the measured result and the fitted curve exceeds the threshold.

frequency components of interference signals' raw SNR. The results displayed in Figure 8 were obtained when LSP was used to determine the spectrum of IMF following decomposition. The results demonstrate that EMD is capable of decomposing signals into their constituent frequency components. Nonetheless, there are still frequency components that are aliased together in a complicated scenario like the ocean. Moreover, more distinction is required. In fact, we have excluded data with heights in the range of 5-10 m when dealing with retreived heights. To show more results, we have kept the LSP spectrum estimates for measured heights in the range of 0-20 m in Figure 8.
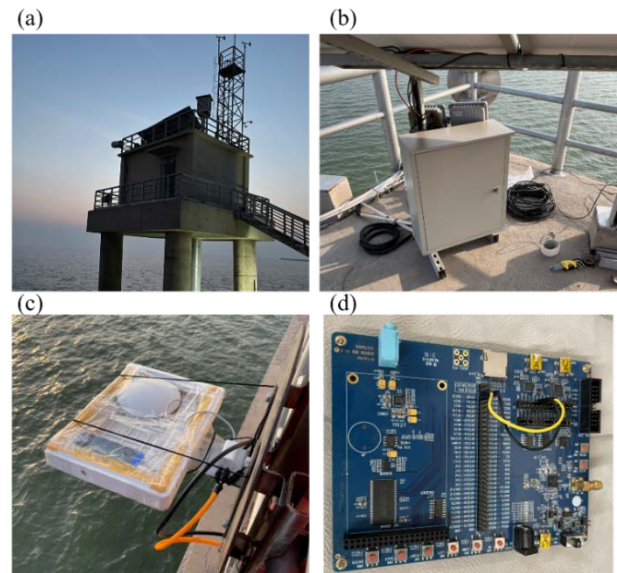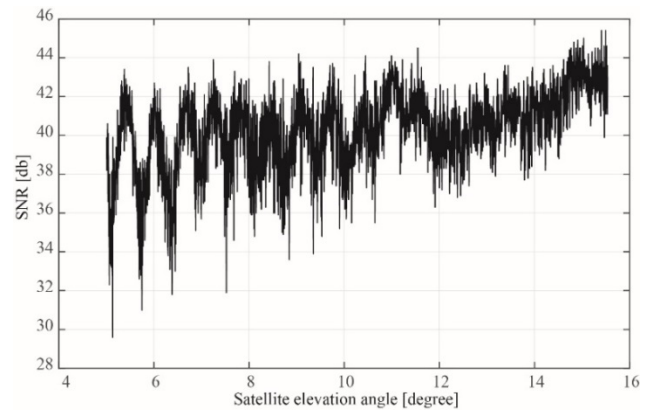

Figure 6 Experiment site

Figure 7 SNR of measured raw interference signal

Using the algorithm in this study, the trend comparison graph between the retrieved and the *in-situ* tide is obtained. As Figure 9 (a) shows that the retrieved and *in-situ* tide have a good agreement. The experimental station's wind speed record is displayed in Figure 9 (b). It is important to note that the measurements differ significantly around November 7. This is because the wind speed is stronger at this time (above 15m/s), which causes the signal character component to weaken and impact the measurement. Finally, the measurement error is shown in Figure 9 (c).

4. Results

To create the scatter plot seen in Figure 10, we use the retrieved tide as the Y-axis and the *in-situ* tide as the X-axis. The results reveal that the points are essentially distributed along the reference line *X=Y*, demonstrating a strong connection between the retrieved and observed tides. The measured and retrieved tides have a 0.89 correlation, and the RMSE is 0.23 m.
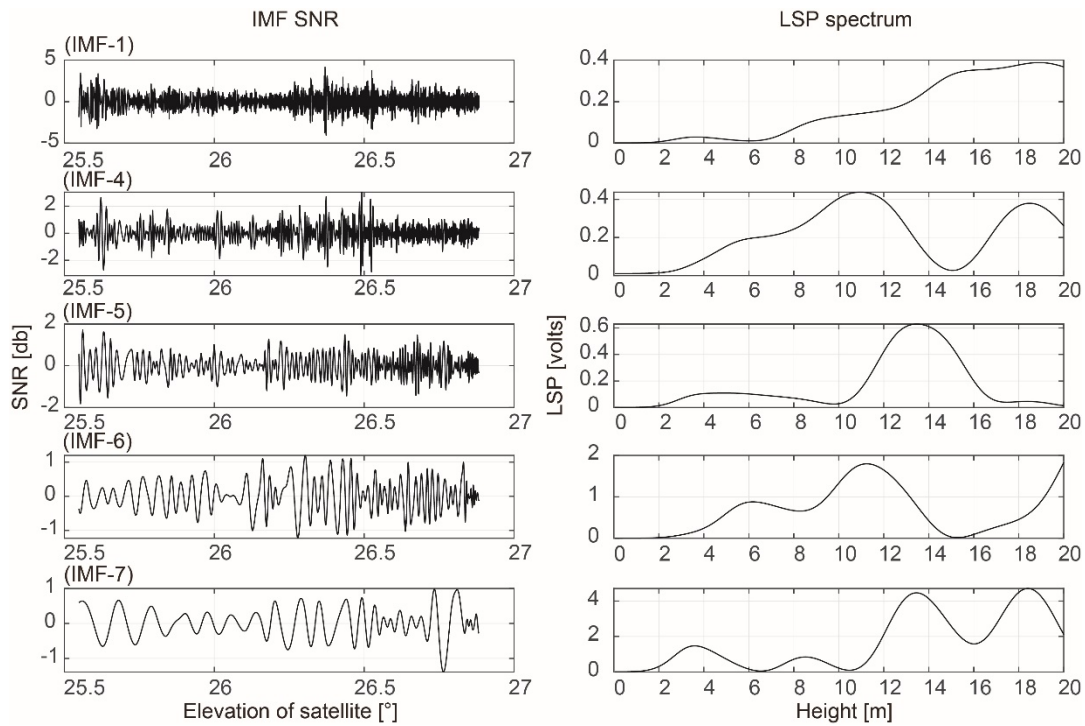

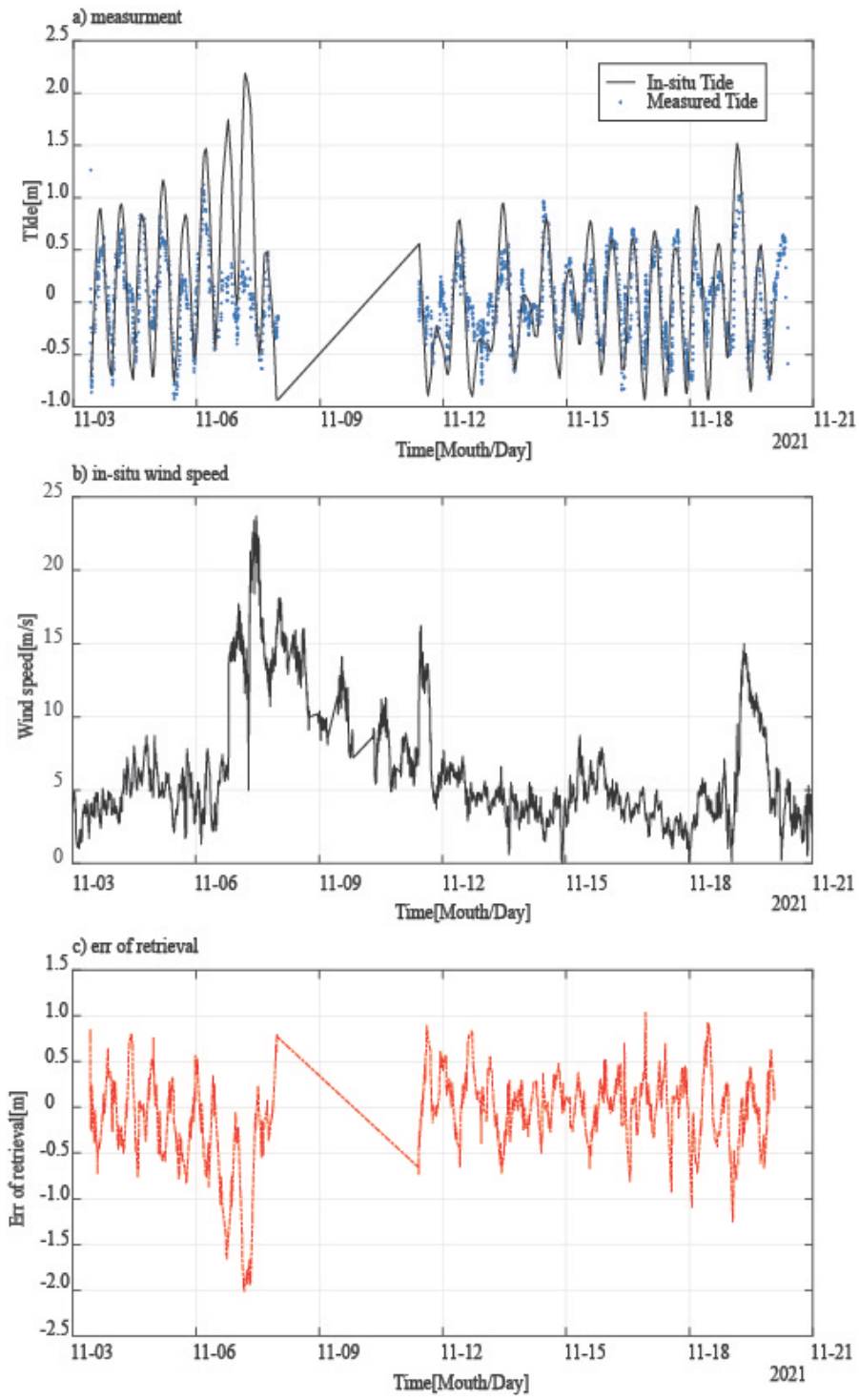Figure 8 IMF and LSP spectrum for raw interference signal SNR

Figure 9 (a) Retrieved and *in-situ* tide change with time, (b) *in-situ* wind speed
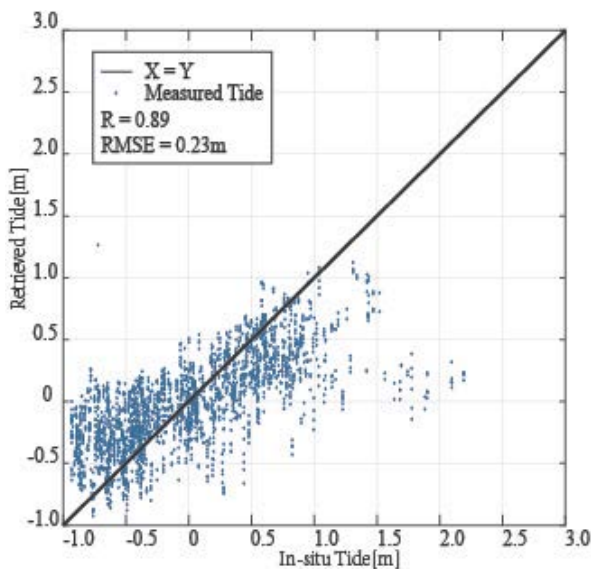
Figure 10 Scatter of retrieved and *in-situ* tide

5. Discussion

Since it was used for ground tracking, GNSS-IR has been extensively used in tide measurement. The benefits of GNSS-IR tide survey over conventional tide survey methods include easy installation and a large measuring window. This paper collects interference signals created by reflected on the sea surface and direct signals and records them in the form of SNR in order to further lower the monitoring cost. This paper's simulation and experiment confirm the viability of using low-cost GNSS receivers for measuring tides, which successfully enables widespread station dissemination.

More precise tide measurement can be obtained at a reduced expense by integrating GNSS-IR altimetry technology with conventional GNSS receivers. Additionally, the time needed to distribute tidal measuring stations based on GNSS-IR can be shortened while reducing the complexity of development. It is a significant area for growth in the realm of remote sensing.

6. Conclusion

There has been extensive usage of GNSS-IR retrieval of in-shore tide variations. In this study, a low-cost GNSS chipset is employed for tidal measurement in an effort to address issues with high cost, challenging large-scale receiver architecture, and the effect of storm surge on inversion accuracy.

In this study, the raw SNR of GNSS interference signals was deposed into its various frequency components using EMD, and the estimated frequencies of the various signals were determined using LSP. In order to completely remove the impact of wild points and storm surge on measurement accuracy, the sinusoidal fitting approach was adopted. The single board utilized in this study costs less than 1000 RMB, and using only one antenna can further cut costs. Also, this inexpensive GNSS receiver and GNSS-IR technology combined can significantly lessen the issues with measurement precision brought on by crustal displacement, which is a common tendency of future growth.

7. Reference

[1]. Ghosh, Surajit & Hazra, Sugata & Nandy, Subrata & Mondal, Partho & Watham, Taibanganba & Kushwaha, Satya. (2017). Trends of sea level in the Bay of Bengal using altimetry and other complementary techniques. Journal of Spatial Science. 63. 1-14. 10.1080/14498596.2017.1348309.

[2]. Zheng, Naiquan & Chen, Peng & Li, Zheng. (2021). Accuracy analysis of ground-based GNSS-R sea level monitoring based on multi GNSS and multi SNR. Advances in Space Research. 68. 10.1016/j.asr.2021.04.024.

[3]. Martin-Neira, M.: A passive reflectometry and interferometry system (PARIS): application to ocean altimetry. ESA J. 17, 331–355 (1993).

[4]. Hong, Xuebao & Zhang, Bo & Geiger, Alain & Han, Mutian & Yang, Dongkai. (2021). GNSS Pseudo Interference Reflectometry for Ground-Based Soil Moisture Remote Sensing: Theory and Simulations. IEEE Geoscience and Remote Sensing Letters. PP. 1-5. 10.1109/LGRS.2021.3068347.

[5]. Larson, Kristine & Small, Eric. (2014). Normalized Microwave Reflection Index: A Vegetation Measurement Derived From GPS Networks. Selected Topics in Applied Earth Observations and Remote Sensing, IEEE Journal of. 7. 1501-1511. 10.1109/JSTARS.2014.2300116.

[6]. Larson, K.M., Gutmann, E.D., Zavorotny, V.U., Braun, J.J., Williams, M.W., Nievinski, F.G.: Can we measure snow depth with GPS receivers? Geophys. Res. Lett. 36, L17502 (2009)

[7]. Reinking, J.. (2016). GNSS-SNR water level estimation using global optimization based on interval analysis. Journal of Geodetic Science. 6. 10.1515/jogs-2016-0006.

[8]. Martin-Neira, M.: A passive reflectometry and interferometry system (PARIS): application to ocean altimetry. ESA J. 17, 331–355 (1993)

[9]. Belmonte Rivas, Maria. (2003). Study on GNSS Carrier Phase for Ocean Altimetry. 10.13140/2.1.1304.0009.

[10]. Wang, Xiaolei & Niu, Zijin & Chen, Shu & He, Xiufeng. (2021). A Correction Method of Height Variation Error Based on One SNR Arc Applied in GNSS–IR Sea-Level Retrieval. Remote Sensing. 14. 11. 10.3390/rs14010011.

[11]. Song, Minfeng & He, Xiufeng & Wang, Xiaolei & Zhou, Ye & Xu, Xueyong. (2019). Study on the Quality Control for Periodogram in the Determination of Water Level Using the GNSS-IR Technique. Sensors. 19. 4524. 10.3390/s19204524.

[12]. Peng, Dongju & Feng, Lujia & Larson, Kristine & Hill, Emma. (2021). Measuring Coastal Absolute Sea-Level Changes Using GNSS Interferometric Reflectometry. Remote Sensing. 13. 4319. 10.3390/rs13214319.

[13]. Dahl-Jensen, Trine & Andersen, Ole & Williams, Simon & Helm, Veit & Khan, Shfaqat. (2021). GNSS-IR Measurements of Inter Annual Sea Level Variations in Thule, Greenland from 2008–2019. Remote Sensing. 13. 5077. 10.3390/rs13245077.

[14]. Sun Xuezhi, Zheng Wei, Wu Fan, et al. Improving the iGNSS-R ocean altimetric precision based on the coherent integration time optimization model[J]. Remote Sensing, 2021, 13: 4715

[15]. Wang, X., Zhang, Q. & Zhang, S. Water levels measured with SNR using wavelet decomposition and Lomb–Scargle periodogram. *GPS Solut* **22**, 22 (2018).

https://doi.org/10.1007/s10291-017-0684-8

[16]. Zhang, Shuangcheng & Liu, Kai & Liu, Qi & Zhang, Chenglong & Zhang, Qin & Nan, Yang. (2019). Tide Variation Monitoring based improved GNSS-MR by Empirical Mode Decomposition. Advances in Space Research. 63. 10.1016/j.asr.2019.01.046.

[17]. Hu, Yuan & Yuan, Xintai & Liu, Wei & Wickert, Jens & Jiang, Zhihao & Haas, Rüdiger. (2021). GNSS-IR Model of Sea Level Height Estimation Combining Variational Mode Decomposition. IEEE Journal of Selected Topics in Applied Earth Observations and Remote Sensing. PP. 1-1. 10.1109/JSTARS.2021.3118398.

Authors

JieLi received his Bachelor's Degree from the School of Electronic and Information Engineering at Harbin Institute of Technology, Harbin, China, in 2016. From 2016 to 2018, he worked with his Master's Degree in Communication and Information Engineering. From 2020, he started pursuing the Ph.D. degree in Communication and Information Systems at Beihang University, Beijing, China. His interest lies in the Global Navigation Satellite System Reflectometry (GNSS-R) application in land observation.

DongkaiYang was born in 1972, in China. He received his BSc. in Electronic Engineering from the North University of China, Taiyuan, China, in 1994, and his MSc. and PhD in Communication and Information Systems from Beihang University, Beijing, China, in 1997 and 2000, respectively. From 2001 to 2002, he was a Research Fellow with the Nanyang Technological University, Singapore. Since 2010, he has been a full-time professor at the School of Electronic and Information Engineering at Beihang University. His interests include the Global

Navigation Satellite System (GNSS) and its applications.

Feng Wang received his Bachelor's Degree from the School of Electronic and Information Engineering at Beihang University, Beijing, China, in 2012. From 2012 to 2014, he worked with his Master's Degree in Communication and Information Engineering. From 2014 to 2019, he began pursuing his PhD. Degree in Information and Signal Processing. In 2020, he started his postdoctoral work at the School of Electronic and Information Engineering, Beihang University. His interest lies in the Global Navigation Satellite System Reflectometry (GNSS-R) application in earth observation.

Jin Xing received his Bachelor's Degree from the School of Information Engineering, China University of Geosciences, in Beijing, China, in 2016. From 2016 to 2019, he worked on his Master Degree in electronic and information engineering at Hainan University. Since 2019, he has been pursuing his PhD. Degree in Information and Signal Processing at Beihang University. His interests include GNSS-R applications in ocean observations